Particle & Particle Systems Characterization

www.particle-journal.com

Doping of Fullerene-Like MoS_2 Nanoparticles with Minute Amounts of Niobium

*Rita Rosentsveig, Lena Yadgarov, Yishay (Isai) Feldman, Sana Shilstein, Ronit Popovitz-Biro, Bojana Visic, Anastasiya Sedova, Sidney R. Cohen, Yuanyuan Li, Anatoly I. Frenkel, and Reshef Tenne**

Inorganic fullerene-like closed-cage nanoparticles of MoS_2 and WS_2 (IF-MoS_2; IF-WS_2), are synthesized in substantial amounts and their properties are widely studied. Their superior tribological properties led to large scale commercial applications as solid lubricants in numerous products and technologies. Doping of these nanoparticles can be used to tune their physical properties. In the current work, niobium (Nb) doping of the nanoparticles is accomplished to an unprecedented low level (≤0.1 at%), which allows controlling the work function and the band gap. The Nb contributes a positive charge, which partially compensates the negative surface charge induced by the intrinsic defects (sulfur vacancies). The energy diagram and position of the Fermi level on the nanoparticles surface is determined by Kelvin probe microscopy and optical measurements. Some potential applications of these nanoparticles are briefly discussed.

1. Introduction

Doping of semiconductors is one of the most fundamental processes for controlling their electrical properties and essential for the fabrication of electronic devices. Substituting one of the atoms in the host lattice with a foreign atom with one extra electron leads to n-type doping, while substitutional dopant atom with one less electron than the host material yields p-type conductivity. Device physics shows that overloading the semiconductor with excess impurity atoms beyond ≈1000 ppm (0.1 at%) is counterproductive; therefore, much lower doping densities are required for the active layer in general.[1] The electronic structure of the outer shell of molybdenum is $4d^5 5s^1$. The number of valence electrons (18) in MoS_2 is sufficient to fill completely the valence band, and thus, MoS_2 is a semiconductor with an indirect gap of 1.23 eV and a direct gap of 1.92 eV at the Γ (gamma) point.[2,3]

Rhenium and halide atoms, being substitutional atoms to the molybdenum and sulfur atoms, respectively, serve as proper n-type dopants for MoS_2 crystals.[4–6] Indeed Re-doping (<1000 ppm) of fullerene-like molybdenum sulfide (IF-MoS_2) nanoparticles (NP) was recently accomplished.[7] This resulted in vastly improved tribological behavior of the NP with friction coefficients nearing the superlubricity regime, offering them applications in a variety of medical technologies.[8] On the other hand, substitution of Mo atoms by Nb atoms in the lattice contributes one extra hole to the valence band of MoS_2 per ionized acceptor state, lending the nanoparticle a p-type character. In the past niobium was found to be the best p-type dopant for this compound.[9–12] More recently, substantial effort has been devoted to the study of the p-type conductivity of MoS_2 obtained by Nb doping, see for example, refs. [13–15]. Theoretical considerations[16–18] showed that the Fermi level of heavily Nb-doped MoS_2 shifts below the valence band maximum and hence leads to excess free (hole) carriers. However, in none of the above works Nb levels below 1000 ppm could be realized in the MoS_2

Dr. R. Rosentsveig, Dr. L. Yadgarov, Dr. S. Shilstein, Dr. B. Visic, A. Sedova, Prof. R. Tenne
Department of Materials and Interfaces
Weizmann Institute
Rehovot 76100, Israel
E-mail: reshef.tenne@weizmann.ac.il

Dr. L. Yadgarov
Schools of Chemistry and Physics
Tel-Aviv University
Tel Aviv 69978, Israel

Dr. Y. (Isai) Feldman, Dr. R. Popovitz-Biro, Dr. S. R. Cohen
Department of Chemical Research Support
Weizmann Institute
Rehovot 76100, Israel

DOI: 10.1002/ppsc.201700165

Dr. B. Visic
Condensed Matter Physics Department
Jozef Stefan Institute
Jamova 39, 1000 Ljubljana, Slovenia

A. Sedova
Nanoscience and Nanotechnology
Cinvestav
Mexico City, P.O. Box 14-740, 07000 México D.F., Mexico

Dr. Y. Li, Prof. A. I. Frenkel
Materials Science and Chemical Engineering Department
Stony Brook University
Stony Brook, NY 11794, USA

lattice, let alone in MoS_2 NPs. Niobium forms stable solid solutions over a wide concentration range, i.e., up to 25 at% in $Nb_xMo_{1-x}S_2$.[17,18] Indeed, reacting a mixture of Nb- and Mo-chlorides with H_2S gave rise to $Nb_xMo_{1-x}S_2$ nanoparticles with Nb concentration of 5–25 at%.[19] Attempts to further reduce the Nb concentration below 1 at% by this methodology were unsuccessful.

The high-temperature synthesis of MoS_2 crystallites leads to sulfur vacancies which are native n-type dopants. This characteristic was confirmed, through zeta potential (ZP) measurements.[20,21] Fullerene-like nanoparticles of molybdenum disulfide (IF-MoS_2) were synthesized by reacting MoO_3 vapor with hydrogen and H_2S at a temperature of 800–840 °C.[22] This high temperature synthesis produced sulfur vacancies in the IF nanoparticle lattice, inducing negative surface charge, also confirmed by zeta potential measurements.[23]

In comparison with Re-doping,[7] the doping of IF-MoS_2 with minute amounts of Nb faced even more daunting challenges. First, the vapor pressure of the different niobium oxide phases is too low at the relevant temperatures to afford congruent evaporation of the molybdenum and niobium oxides. For example, niobium pentoxide does not have an appreciable vapor pressure even at 1350 °C. Since congruent evaporation of the Nb-oxide with the majority phase MoO_3 could not be achieved at the relevant range of temperatures for the IF NP production (800–900 °C), an alternative synthetic strategy was developed for preparing niobium doped IF-MoS_2 using a mixed Mo—Nb-oxide as a precursor.

Furthermore, due to its low content (<0.1 at%), quantitative analysis of the Nb concentration in the IF-MoS_2 nanoparticles could not be realized using the standard techniques, such as X-ray diffraction (XRD), energy dispersive X-ray analysis (EDS), or photoelectron spectroscopy (XPS). Inductive-coupled plasma mass spectrometry (ICP-MS), which was used to determine the Re content in IF-MoS_2,[7] was found to provide erroneous data (see details below). Fortunately, in the present work resonance X-ray fluorescence (XRF) could be applied to determine the Nb content at a level of <0.1 at%. Generally, this method is less accurate than ICP-MS but was definitely more reliable in the present case.

Kelvin probe force microscopy (KPFM) provides a noncontact and noninvasive mapping of the local surface electric potential, which is the contact potential difference (CPD) due to the difference in work functions between the sample surface and the tip.[24,25] The work function is affected by the surface electrical properties, such as dielectric constants, surface charges, and doping levels. Here, KPFM was used to study the difference in the work functions of the Nb-doped and undoped IF.

In this paper niobium doping of IF-MoS_2 nanoparticles at concentrations of about 1000 ppm (0.1 at%) is reported. A new synthetic procedure incorporating Nb—Mo-oxide precursor was used for this reaction. Although Nb-doping of MoS_2 in the form of 2D crystalline material and single crystals has been reported previously, this work demonstrates the doping of nanoparticles. In particular, the low Nb concentrations achieved here were not reached in those earlier works. Furthermore, a new analytical methodology was developed to determine the Nb content of the nanoparticles. Some physical measurements characterizing the doped nanoparticles are described, as well. As expected, the density of (negative) charge at the surface of the nanoparticles was reduced compared to the undoped IF-MoS_2 nanoparticles at pH 7. However, full conversion of the negative surface charge to positive charge was, so far, not accomplished. The full band-diagram of the nanoparticles prior to and after the Nb-doping is presented. The synthetic strategy used for the niobium doping of fullerene-like nanoparticles of MoS_2 can, with some modifications, be adapted also for the doping of WS_2 nanoparticles and inorganic nanotubes of WS_2 and MoS_2.

2. Experimental

The reactor for the synthesis of the Nb:IF-MoS_2 NPs is based on a previous study with appropriate modifications.[7,22] However major changes in the preparation of the oxide precursor and the analytical tools to quantify the Nb-concentration were required in order to achieve a controlled Nb doping (≤1000 ppm) of the IF-MoS_2 nanoparticles. Furthermore, much higher synthetic temperatures were used in order to evaporate the mixed niobium-molybdenum-oxide. Each of these three points, which are discussed in detail below, required a lengthy effort in order to establish a reproducible strategy for the synthesis of the Nb-doped IF nanoparticles.

2.1. Preparation of the Precursor

The precursor for the doped IF nanoparticles was the mixed phase $Nb_2Mo_3O_{14}$. Much of the synthetic effort was focused on controlling the reaction parameters of the auxiliary reactor for preparing the mixed oxide phase. This latter tetragonal phase revealed quite significant deviations from stoichiometry (see below), which could not be easily controlled for the follow-up (sulfidization) reaction.

The tetragonal mixed niobium-molybdenum-oxide phase was prepared via a solid-state reaction using high purity grade oxides from Aldrich. Weighted powders of MoO_3 (99.5%) and Nb_2O_5 (99.9%) in molecular ratio 3:1 were ground and mixed carefully in air. The powder was then inserted into quartz crucibles and placed in a quartz reactor (**Figure 1**a) under nitrogen gas flow. The reactor was purged continuously with N_2 in order to prevent traces of O_2 and moisture that would otherwise interfere with the course of the reaction. Following this step the reactor was inserted into a horizontal furnace which was preheated to 700 °C and maintained at this temperature for 16–18 h. Following this, the boat with crucibles containing solid-solution "cake" was moved out of the oven and left to cool to room temperature.

2.2. Synthesis of the Nb:IF-MoS_2

The subsequent conversion of the pre-prepared sintered Nb—Mo-oxide cake into the Nb doped IF-MoS_2 nanoparticles (Nb:IF-MoS_2) was carried out in a vertical quartz reactor, used previously for the synthesis of undoped IF-MoS_2[22] (see Figure 1b). The present synthesis bears some similarity to that of IF-MoS_2. However higher temperatures were required here,

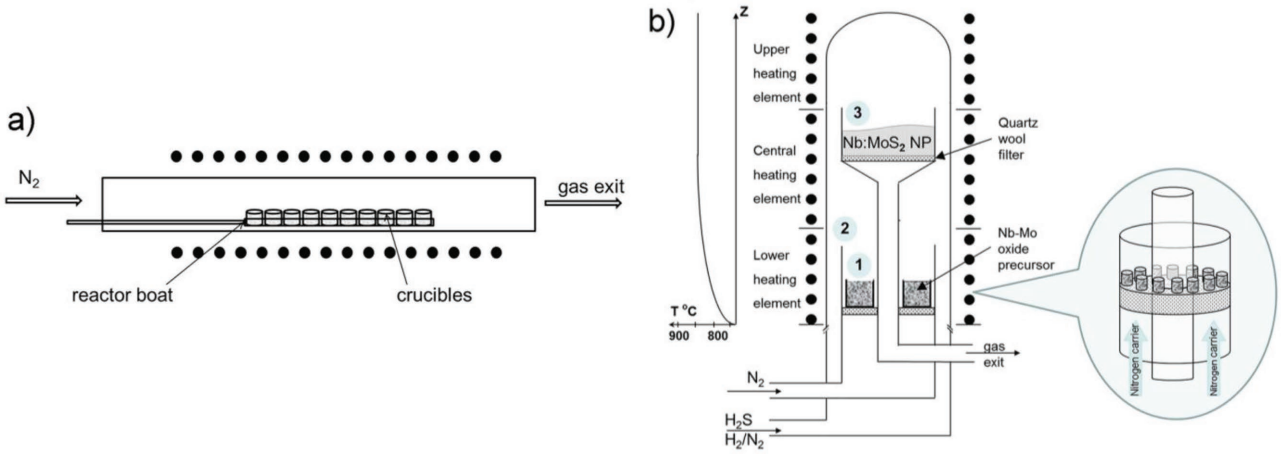

Figure 1. a) Reactor for the preparation of the niobium-doped molybdenum oxide (Nb—Mo-oxide) precursor "cakes." b) Modified quartz reactor used for the synthesis of the Nb:IF-MoS_2 NP with the temperature profile shown along the reactor (*z*) axis, on the left. Numbers 1–3 represent the different reaction zones (see text).

which made exquisite control over the morphology of the IF nanoparticles and their Nb-content much more difficult. The entire synthesis could be separated into four consecutive steps:

1. Evaporation of the Nb—Mo-oxide cake at a temperature of about 810 °C (zone 1)
2. Partial reduction of the oxide vapor with consequent condensation of the reduced vapor into Nb-doped MoO_{3-y} nanoparticles (zones 1 & 2)
3. Fast sulfidization of the first few layers of the oxide nanoparticles in the volume of the reactor (zone 2)
4. Further sulfidization of the nanoparticles proceeding on the collecting quartz wool filter (zone 3)
5. Final annealing of the powder in the presence of H_2S/H_2 at 870–900 °C for 35–40 h.

The first step is new, while the synthesis of the Nb-doped IF nanoparticles (steps 2, 3) was carried-out at higher temperatures than those used for undoped IF-MoS_2. The higher temperature was required due to the lower evaporation rate of the mixed Nb—Mo-oxide. The temperature in zone 1 was kept around 810 °C (vs about 760 °C for the undoped IF-MoS_2). The increased reaction temperature resulted in faster reaction dynamics, making it more difficult to control the IF morphology.

All the crucibles were weighed before and after the synthesis and the amount of the evaporated phase was determined by the weight difference. The average evaporation rate was 1.5–3.5 mg min^{-1} (vs 5.5–7.5 mg min^{-1} for the undoped IF-MoS_2 synthesis).

2.3. X-ray Diffraction; X-ray Fluorescence and Electron Microscopy of the Precursor and Product

All the specimens were investigated by recording their X-ray powder patterns in an X-ray diffractometer (XRD-Ultima-III, Rigaku). Transmission electron microscopy (TEM) analysis, electron diffraction, and EDS measurements were performed with a Philips CM120 microscope operating at 120 kV and equipped with a EDS analyzer (EDAX Phoenix Microanalyzer) and with a Jeol2100 microscope operating at 200 kV, equipped with a Thermo Fisher EDS analyzer. High resolution TEM (HRTEM) images were recorded with a Tecnai F30 UT (FEI) microscope operating a 300 kV, see also Section 1.1 of the Supporting Information. For the scanning electron microscopy (SEM), Zeiss Ultra model V55 and LEO model Supra 55VP equipped with EDS detector (Oxford model INCA) and backscattering electron (BSE) detector were used.

Unfortunately, in the present study, ICP-MS provided erroneous data of the niobium concentration in the oxide and sulfide matrices (see details below). Thus, for determining the Nb level in the MoS_2 nanoparticles, resonance XRF was performed using an X-Ray fluorescent spectrometer EX-CALIBUR. The X-ray source was a molybdenum tube (45 keV) and the beam diameter was 2 mm. For a detailed description of the resonance XRF analysis see Section 1.2 of the Supporting Information. This technique was found to be the most reliable in the present case. In fact the XRF analysis for such samples could not be used to determine the Nb concentration below 0.02 at% (200 ppm) and was thus approximately one order of magnitude less accurate than ICP-MS analysis.[7]

2.4. X-ray Absorption Fine Structure (XAFS) Analysis

To determine the location of doped Nb atoms in the IF-MoS_2 lattice and their coordination with the neighboring sulfur atoms, the local structures around Nb and Mo atoms were evaluated by X-ray absorption fine structure (XAFS) measurements. The Nb and Mo K edge XAFS data of Nb:IF-MoS_2 were collected at beamline X18-A, National Synchrotron Light Source, Brookhaven National Laboratory. For these analyses, a sample with 0.11 at% niobium content was used. The sample powder was spread onto an adhesive tape, which was then folded several times and mounted onto the sample stage. The Nb K edge data were collected in fluorescence mode and the Mo K edge data were recorded in transmission mode. For the sake of comparison, the Nb edge data of NbS_2 and Nb foil were collected.

2.5. Zeta Potential Measurements

The surface charge of the undoped and Nb doped nanoparticles was determined through ZP measurements using ZetaSizer Nano ZS (Malvern Instruments Inc, UK) with a He–Ne light source (632 nm). To prepare the samples for these measurements, IF nanoparticles (0.6 mg) were deagglomerated in 20 mL purified water by sonicating for 3–5 min using an ultrasonic bath. Subsequently, 0.2 mL of the IF suspension was added to 1.5 mL aqueous solution with pH varying from 1 to 12, and sonicated for an additional 5 min. Before the addition of IF, the pH of each solution was adjusted using concentrated NaOH or HCl. The final concentration of the IF was 0.004 mg mL^{-1}. The solutions were measured in a folded capillary cell (DTS1060) made from polycarbonate with gold plated beryllium/copper electrodes.

2.6. Scanning Kelvin Probe Force Microscopy Analysis

KPFM is a high-resolution tool used to measure the local contact potential between the atomic force microscope (AFM) nanoprobe and the surface of the sample. The signal is recorded relative to the scanning tip. Thus, we can use the Au film substrate as a reference to which the doped and undoped NPs are compared. A negative signal means a lower work function than the substrate, i.e., electrons would tend to flow from the NP to the substrate.[24–27]

A commercial AFM from AIST-NT Company was used for the AFM/scanning kelvin probe microscopy (SKPM) measurements. A Pt-coated silicon cantilever probe (ANSCM-Pt, APPNano, Mt. View, USA) was used as the conductive probe with a force constant of ≈2 N m^{-1} and a nominal resonance frequency of 60 kHz. Measurements were made in the 2-pass FM mode, with lift height of 60 nm for the second pass. The nanoparticles were placed on a silicon wafer (Sigma-Aldrich) covered by a 200 nm thick Au film sputtered in a vacuum chamber. The microscope was operated in an environmental chamber under temperature of 12 ± 2 C, and controlled humidity (<≈9%). To obtain reliable statistics, 95 doped and 12 undoped NPs were analyzed. The Au substrate was the same for all the samples and consequently could be used as a reference. For further information, see Section 3 in the Supporting Information.

2.7. Absolute Absorption Measurements

The samples were prepared by adding 0.6 mg of the nanoparticles into 9 mL of purified water. The mixture was hand-shaken and then sonicated twice for 1–3 min using an ultrasonic bath. All suspensions were measured using quartz cuvettes. SEM and TEM analyses demonstrated that the IF NPs remain unaffected by this mild sonication procedure.

Decoupled absorption spectra are used to separate out scattering and absorption processes from the total extinction spectra. The net absorption was measured using a Hamamatsu Quantaurus absolute QY system.[28,29] This instrument directly measures the amount of absorbed light by placing the sample inside an integrating sphere. The system was calibrated using a sample with known absorbance in order to extract the optical absorbance. A calibration for counting the single-pass absorption photons was performed to avoid the full extinction, which also includes photons that are scattered a few times before being detected.

The direct transition was determined from the Rydberg formula: $E_{g,dir} = E_A + E_{Ryd}$, where E_A is the A-exciton energy, and $E_{Ryd} = 0.042$ eV is the exciton Rydberg constant.[30] The indirect gap was calculated from the formula: $\alpha = \frac{A(h\nu - E_g)^n}{h\nu}$. Here α is the absorption coefficient, A is a constant, E_g is the indirect band gap (BG) of the semiconductor and $n = 1/2$.

3. Results and Discussion

3.1. Synthesis and Characterization of the Mixed Nb-Mo-O Precursor

Mixed Mo—Nb-oxide phases have been described in the literature.[31–34] All of them contain a high fraction of Nb. Among several Nb—Mo mixed oxides, the tetragonal $Nb_2Mo_3O_{14}$ phase, which is relatively well studied,[31] was chosen as a possible precursor for the present synthesis. Numerous experiments were carried out to establish the desirable strategy for the preparation of the oxide precursor. Following the reaction at 700 °C, a careful analysis of the phases and the composition of the cake were undertaken by XRD, XRF, SEM/EDS, and TEM/EDS/ED. The composition of the cake and the Nb/Mo ratio were found to vary appreciably as a function of depth below the surface. Quantitative evaluation of the oxide composition in the cake and the Nb/Mo ratio was therefore undertaken. For that purpose, seven successive layers about 0.8 mm thick, each, of oxide cake were peeled-off carefully starting from the surface inward. Each peeled layer was carefully ground and then analyzed by both XRD and XRF (see **Figure 2**a and **Table 1**).

The XRD analysis showed that the topmost portion layer of the cake consisted of a pure tetragonal $Nb_2Mo_3O_{14}$ phase. The orthorhombic MoO_3 phase was absent from the first layer (surface of the cake) and was gradually enriched going downward (deeper) into the cake up to a saturation value of 23–24 at%. Figure 2a shows the XRD pattern of three (1st, 2nd, and 4th) peeled layers from the top surface of the oxide cake downward. The top layer (#1) contained exclusively the tetragonal $Nb_2Mo_3O_{14}$ phase. The schematic structure of this tetragonal phase is displayed in the inset of Figure 2a. The lattice parameters of the tetragonal $Nb_2Mo_3O_{14}$ are: $a = 23.15$A; $b = 23.15$A; $c = 4.0$A; alpha = beta = gamma = 90°. It belongs to the space group *P4/mbm* (127). The deeper layers of the cake contained increasing fractions of the orthorhombic MoO_3 phase (cell parameters 3.954 × 13.825 × 3.694; space group *Pbnm* (62)). The results of the XRD analysis are summarized in Table 1. They indicate that the surface layer of the cake is free of MoO_3, likely due to the greater volatility of this phase at 700 °C. This analysis shows also that from the fourth layer and deeper into the bottom of the cake, the ratio between the tetragonal $Nb_2Mo_3O_{14}$ and the orthorhombic MoO_3 phases remained more or less constant, i.e., $3_{tetragonal}$:$1_{orthorhombic}$. Notwithstanding the large deviations from stoichiometry of the

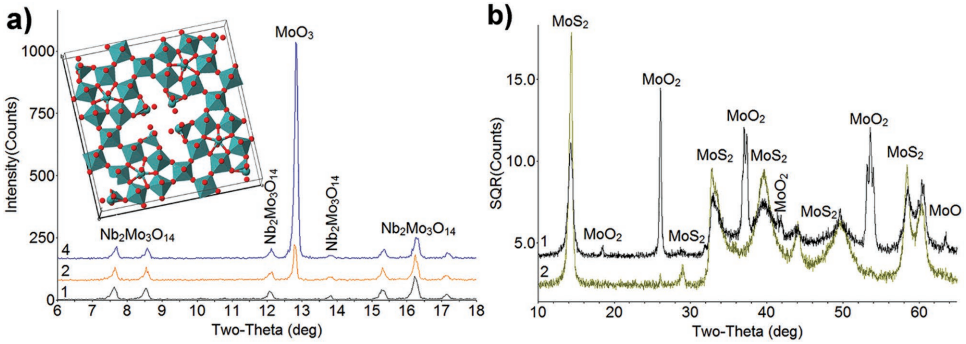

Figure 2. Results of XRD analysis: a) XRD pattern of three (1st, 2nd, and 4th) peeled layers from the top surface of the oxide cake downwards and b) the IF-MoS_2 nanoparticles before (1) and after annealing (2). The inset in (a) shows the crystalline structure of the tetragonal $Nb_2Mo_3O_{14}$ phase along the *c*-axis.

tetragonal phase (see below) the lattice parameters of this phase remained the same all along the cake depth, which apparently is typical for these compounds.[35]

The Nb/Mo ratio was evaluated also by resonance XRF (Table 1). The XRF analysis revealed a complex distribution of the elements in the tetragonal phase. Formally, the Nb/Mo ratio is given by the ratio $[Nb_{Nb2Mo3O14}]/[Mo_{Nb2Mo3O14+MoO3}]$. Thus, the surface layer which consisted of a purely tetragonal phase, as determined by XRD, should follow the ratio between the two elements in this phase. Despite this, the Nb ratio in the surface layer, was far higher (0.93) than expected, i.e., 0.66. This finding suggested that the tetragonal phase can suffer large deviations from stoichiometric composition. In fact the Nb/Mo ratio throughout the depth of the cake was always larger than the expected 0.66 ratio and as of the fourth layer showed a stable ratio of 0.77. This large deviation from stoichiometry could be the manifestation of the excess volatility of MoO_3 phase during the 16 h annealing at 700 °C.

TEM analysis was undertaken in order to further understand the complex relationship between the niobium and molybdenum in these oxide phases. The details of the TEM analysis of the oxide precursor are provided in Section 1.1 of the Supporting Information. This analysis showed in general larger than expected (0.66 ratio) excess of niobium in the tetragonal phase. Furthermore, the Nb/Mo ratio varied from 0.61 to 1.72 and considerable variations were recorded from one crystallite to the other. However, the lattice parameters of this phase, which were determined by electron diffraction, were in agreement with the XRD values of the tetragonal $Nb_2Mo_3O_{14}$ phase.

The present results could be rationalized by proposing a substitution of Mo^{6+} ions by Nb^{5+} ions in the tetragonal lattice. A previous study of the crystal structure of $Nb_2Mo_3O_{14}$ using the anomalous X-ray scattering of synchrotron radiation established the nonordered displacement of Nb and Mo ions in this lattice.[35] In this work some substitution of Nb^{5+} ions by Mo^{6+} ions was observed. In fact, here the opposite situation—substitution of Mo^{6+} by Nb^{5+}—was found, leading to Nb-excess and a large deviation from stoichiometry in this phase. In conclusion, while the present investigation of the mixed niobium-molybdenum-oxide phase describes an intermediate procedure in the synthesis of niobium-doped IF-MoS_2 nanoparticles, it is also of scientific and technological merit on its own.

Table 1. Results of XRD and XRF analyses of the heated oxide mixture from top to bottom.

# Layer (top to bottom)	_1	_2	_3	_4	_5	_6	_7
Nb/Mo atomic ratio, XRF	0.93	0.85	0.7	0.77	0.75	0.77	0.78
MoO_3, wt%, XRD	0	5.9	19.7	23.5	23.5	24.8	22.6
$Nb_2Mo_3O_{14}$, wt%, XRD	100	94.1	81.3	76.5	76.5	75.2	77.4

3.2. Synthesis and Characterization of the Nb-Doped IF-MoS_2 Nanoparticles

3.2.1. Parameterization of the Reaction Conditions

In the first step of the IF-MoS_2 synthesis, the cake was heated to 810 °C and the Nb—Mo-oxide evaporated. The gas phase reaction with hydrogen leads to partial reduction and condensation of Nb—Mo sub-oxide. In the next step, the Nb—Mo sub-oxide NP reacted with H_2/H_2S gas at ≈820 °C converting the surface into a closed sulfide layer. The synthesized nanoparticles were collected on the quartz wool filter (zone 3 in Figure 1b). The process resulted in the synthesis of Nb-doped nanoparticles with 5–10 closed MoS_2 layers engulfing the (Nb-doped) molybdenum dioxide core. The powder was collected from the surface of the filter. A long (35–40 h) annealing of these NPs ensued at 870 °C in the presence of H_2S. The annealing led to a complete conversion of the oxide core into Nb-doped IF-MoS_2 NP. The overall yield of the oxide to sulfide conversion process is close to 50%. That is to say that the ratio of the sulfide is about 50% of the theoretical (stoichiometric) yield, which was calculated based on the oxide weight loss of the cake. Part of the oxide vapor failed to undergo the conversion to sulfide, and was flushed out of the reactor with the gas flow. Furthermore, 70% of the sulfide powder consists of Nb-doped IF-MoS_2 (<200 nm), the rest being mostly large (>300 nm) IF and platelets of 2H-MoS_2 crystallites (see **Figure 3**a and Sec. 3.2.3).

The most important difference between the synthesis of Nb-doped IF-MoS_2 compared to that of undoped IF-MoS_2 is the higher temperature required to evaporate the mixed niobium-molybdenum oxide, i.e., 810 °C (zone 1 in Figure 1b) versus about 760 °C for the undoped syntheses. The higher temperatures are attributed to the much smaller rate of evaporation

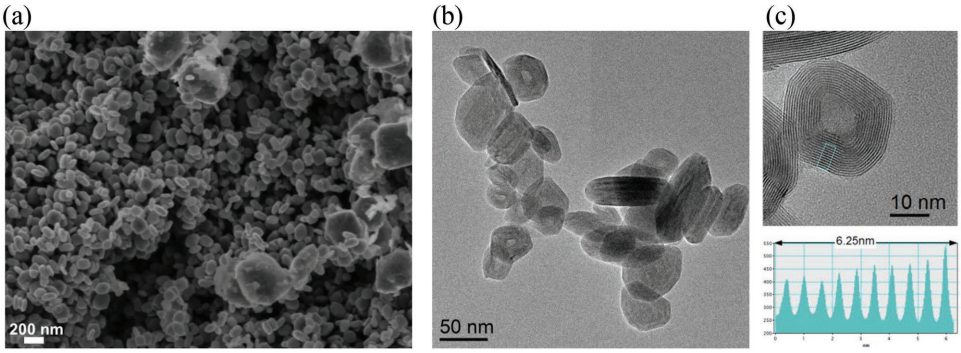

Figure 3. a) SEM and b) TEM micrographs of group of Nb-doped IF-MoS_2 and c) HRTEM of single particle (The interlayer spacing between fringes is shown by the line profile (on the bottom) and is 0.63 nm). Please note that these pictures do not represent the entire product. Only about 70% of the product is high quality IF nanoparticles, the remain being larger IF nanoparticles and platelets of MoS_2.

of the Nb—Mo-oxide. The rate of the oxide evaporation was determined by weighing the crucibles (with the oxide cake) before and after the synthesis. The amount of the evaporated phase was determined by this weight difference. The average evaporation rate was 1.5–3.5 mg min^{-1} (vs 5.5–7.0 mg min^{-1} in the case of undoped and Re:IF-MoS_2). After tedious optimization of the synthetic procedure, the total amount of Nb:IF-MoS_2 nanoparticles was only about 0.5 g for one month of continuous work, which reflects the great difficulty of pursuing this synthesis. The higher temperature used in this reaction resulted in much lower yield of the Nb-doped IF-MoS_2 compared to the undoped NP (see Sec 3.2.3).

3.2.2. X-ray Diffraction Analysis

The results of the XRD analysis are summarized in Figure 2b. The results (curve 2) clearly show that, following the sulfidization reaction and annealing, the oxide nanoparticles have been fully converted into MoS_2 nanoparticles, while the nonannealed nanoparticles (curve 1) are only partially converted into molybdenum sulfide. Remains of the MoO_2 core (≈1%) are then still visible after 30 h annealing at 870 °C (curve 2).

3.2.3. Electron Microscopy Analysis of the Product

The SEM (Figure 3a) and TEM (Figure 3b,c) analysis revealed that the Nb doped IF-MoS_2 phase looks the same as the undoped ones. The interlayer spacing (0.63 nm) was found to be the same as for the undoped NP. Analysis of the SEM/TEM images (a few thousand nanoparticles analyzed) revealed a bimodal size distribution of 20–50 nm and 150–200 nm. The yield of the IF nanoparticles with these sizes was 70%, the remainder being much larger nanoparticles and microscopic platelets. This yield is appreciably lower than for the case of the undoped IF-MoS_2.

3.2.4. Analysis of the Nb Content in the Product

The analysis of minute amounts of the dopant atoms (<0.5 at%) in the nanoparticles is challenging. The XRD pattern of Nb-doped IF-MoS_2 was indistinguishable from that of pure IF-MoS_2 and accordingly, this method (and others like EDS, XPS) was not suitable for monitoring the Nb doping level under different synthetic conditions. Previously, the Re-level in the IF-MoS_2 nanoparticles was determined using mostly ICP-MS analysis.[7] In general, ICP-MS is known to be the most appropriate technique for sub-trace quantitative analysis and identification of the concentration of heavy atoms used as dopants. However, here the ICP-MS technique was unable to accurately identify and determine the Nb concentration due to the fact that: (1) Nb detection is subject to interference from hydrides of Mo, (2) the Nb is adjacent to Mo in the periodic table (similar atomic mass), and since the Mo concentration is much larger than that of Nb, the Mo signal masks the Nb reading. Therefore, determination of the Nb content in IF-MoS_2 was carried out by XRF. This analysis shows that all samples synthesized by the present method contain about 0.03–0.3 at% Nb (see Sec. 1.2 of the Supporting Information for further information on the XRF analysis).

3.2.5. XAFS Analysis

As presented in **Figure 4**a, the normalized Nb K edge X-ray absorption near edge structure (XANES) spectrum of Nb:IF-MoS_2 has spectral features very similar to those of NbS_2, except for the less pronounced shoulder peak at about 18998 eV. Fourier transform magnitudes of the Nb K-edge and Mo K-edge of the extended X-ray absorption fine structure (EXAFS) data of the Nb:IF-MoS_2 and the NbS_2 standard (Figure 4b) all show distinct peak at about 1.8 Å, which originates from Nb—S and Mo—S contributions, respectively. Compared to NbS_2, the Nb—S peak position in Nb:IF-MoS_2 sample shifts toward lower R and is closer to that of the Mo—S peak in the same sample. These observations, confirmed by quantitative analysis described below, indicate that Nb substitutes for Mo (Nb_{Mo}) in Nb:IF-MoS_2.

The extended X-ray absorption fine structure (EXAFS) data were analyzed in order to obtain quantitative information on the local structure around Nb and Mo atoms in Nb:IF-MoS_2. For fitting Nb edge data, a theoretical model was constructed with the X-ray absorbing Nb atom substituted for the Mo atom in the lattice of MoS_2. The FEFF6 program[36] was used to calculate the theoretical EXAFS contribution of the first nearest

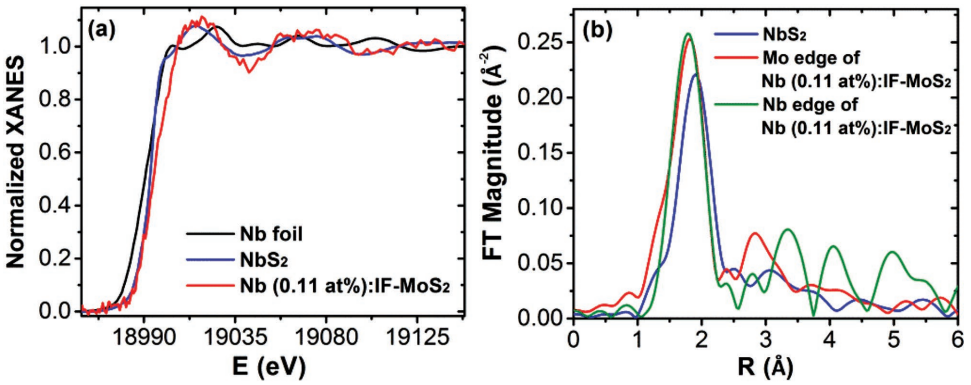

Figure 4. XAFS data of the Nb doped IF-MoS_2: a) the normalized Nb K edge XANES spectrum of Nb:IF-MoS_2 compared to standards of compared to standards of NbS_2 and Nb foil. b) Fourier transform magnitudes of the Nb K-edge and Mo K-edge EXAFS data of the Nb:IF-MoS_2 and the NbS_2 standard.

neighbor (1NN) Nb—S bond. For Mo edge data, the contribution from the 1NN Mo—S bond and 2NN Mo—Mo bond was calculated. The passive electron reduction factors (S_0^2), corresponding to the Mo and Nb EXAFS data of Nb:IF-MoS_2, were obtained from the fits of EXAFS spectra of Mo and Nb foils, and fixed as 1.03 and 0.93, respectively. For Nb—S pairs, coordination number (N), bond distance (R), disorder factor (σ^2), and energy shift (ΔE_0) were varied in the fits. The best fitting results are listed in **Table 2**. For Nb edge spectrum, the fitting k-range is 2.0–9.5 $Å^{-1}$ and the R range is 1.7–2.9 Å. For the Mo edge spectrum, the fitting k-range is 2.0–18.0 $Å^{-1}$ and the R range is 1.0–3.2 Å.

The bond distance of Nb—S is 2.467 Å in the NbS_2 lattice, whereas the bond distance of Mo—S is 2.408 Å in the MoS_2 lattice. According to the results of the fitting of the EXAFS shown in Table 2, the Mo—S bond distance in Nb (0.11 at%):IF-MoS_2 (2.406 Å) is very close to that in bulk MoS_2. The Nb—S bond distance in Nb:IF-MoS_2 (2.418 Å) lies between that of Mo—S in the bulk MoS_2 and Nb—S in the bulk NbS_2 (2.47 Å), which is expected if Nb substitutes for Mo in Nb:IF-MoS_2.

Table 2. Best EXAFS fitting results for Nb (0.11 at%):IF-MoS_2. The EXAFS fitting results for NbS_2 reference are also listed for comparison.

Nb (0.11 at%):IF-MoS_2		
Bond	Coordination number [N]	Bond distance (R) [Å]
Mo—S	5.6 ± 0.3	2.406 ± 0.004
Mo—Mo	5.1 ± 0.7	3.159 ± 0.005
Nb—S	4.9 ± 2.2	2.418 ± 0.029
NbS_2 reference		
Bond	Coordination number [N]	Bond distance (R) [Å]
Nb—S[a)]	6	2.47
Nb—S[b)]	3.4 ± 0.7	2.484 ± 0.013

[a)]EXAFS fitting results for bulk NbS_2: reproduced from ref. [37]; [b)]EXAFS fitting results for synthesized NbS_2: The lower coordination number of Nb—S was attributed to niobium excess and the reported intercalation of Nb between the NbS_2 layers.[38]

3.2.6. Zeta Potential Analysis

The effect of doping on the surface charge of the IF nanoparticles was studied using ζ-potential (ZP) measurements. Here, the ZP of the undoped and Nb doped IF-MoS_2 was measured as a function of pH and is presented in **Figure 5**. The calculated ZP values are based on a model which considers colloidal solutions of spherical NP. Since the 2H-MoS_2 platelets are not spherical and tend to sediment out after a few minutes, their surface potential could not be measured by this method.

Both the undoped and Nb doped NPs form relatively stable colloidal suspensions and do not precipitate for a few hours in the pH range of 5–12. Moreover, the negative ZP of the doped and undoped IF NP remains almost unchanged in this pH range. This behavior implies that in neutral solution the IF NPs acquire high negative surface charge which is probably associated with adsorbed moieties at the intrinsic defects of the curved MoS_2 layers of the NP. Above pH 12, the ionic strength is too high and the Debye screening length too low to afford

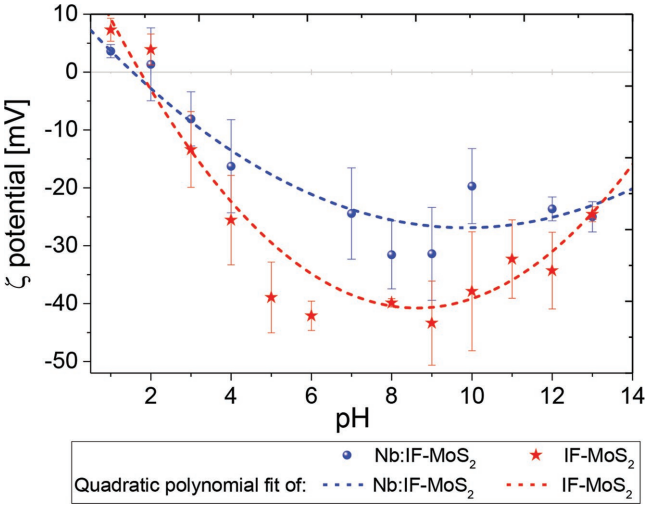

Figure 5. Zeta potential versus pH for Nb doped and undoped IF-MoS_2 nanoparticle dispersed in water. The dotted lines were obtained by polynomial fit and are used to guide the eye.

stable NP suspensions. In the pH range below 5 the ZP rapidly increases with decreasing pH, i.e., the surface charge of the NP is too low to impart sufficient self-repulsion resulting in a rapid agglomeration without stirring.

The ζ-potential values of the undoped NP are appreciably higher (more negative) than the Nb-doped NP in the pH range 5–12 (Figure 5). The results of the ZP measurements suggest that although all the examined NPs possess negative surface charges, the Nb-doped NP is less negative, i.e., diminished n-type character. For instance, at pH = 7, the ZP is −38.5 and −24.2 meV, respectively, for undoped and Nb doped IF-MoS_2. Namely, the substitutional Nb doping partially "anneals-out" the negative surface charge of the NP. Interestingly, all the measured NPs have very similar isoelectric point, i.e., pH ≈ 1.7. This underscores the remaining structural similarities between all the NPs.

3.2.7. Kelvin Probe Measurements

The KPFM images are presented in Figure S4 (Supporting Information) together with the simultaneously acquired topographies, yielding both NP morphology and local surface potentials. The particle shape and size are in good agreement with TEM/SEM images. Both doped and undoped NPs in KPFM images consistently appeared darker in color with respect to the substrate (gold) background. This is consistent with negatively charged NPs. The CPD values correlate with geometry (aspect ratio), but the variation even for similarly shaped NPs indicates different degree of doping for individual NPs. For instance, for the Nb:IF-MoS_2 with diameter of 20 nm, the CPD shift varies by ≈260 meV (from −115 to −380 meV). Statistics of CPD values for all the measured NPs can be found in Sec. S3.2 of the Supporting Information (Figure S5, Supporting Information). The statistical analysis showed that there is a significant difference between the CPDs of doped and undoped NPs. Size-averaged CPDs of the NPs are −240 ± 45 meV for the Nb doped IF and −550 ± 42 meV for the undoped IF-MoS_2. Pooled variance *t*-test confirmed that these are two distinct populations (t = 23). This finding substantiated the modification of NP electronic properties through substitutional Nb doping, whereby the smaller (less negative) CPD of the Nb doped IF coincides with the theoretical predictions that niobium doping will induce p-type behavior.[11]

3.2.8. Absorption Measurements and Optical Transitions

The comparison between the absorption spectra of the bulk (platelets) 2H-MoS_2, undoped, and Nb doped IF-MoS_2 nanoparticles are shown in **Figure 6**. The spectra show the typical long wavelength absorption (>740 nm) due to the indirect transition; the sharp rise due to the direct transition in the *K*-point of the Brillouin zone; the A and B excitonic peaks at 680 and 630 nm and the broad C-exciton absorption with peak at 500 nm. **Table 3** summarizes the different transitions and calculated band gap in comparison to the values calculated for the undoped Re-and Nb-doped IF-MoS_2 nanoparticles and the bulk. In accordance with past studies, the band gap of the IF nanoparticles is

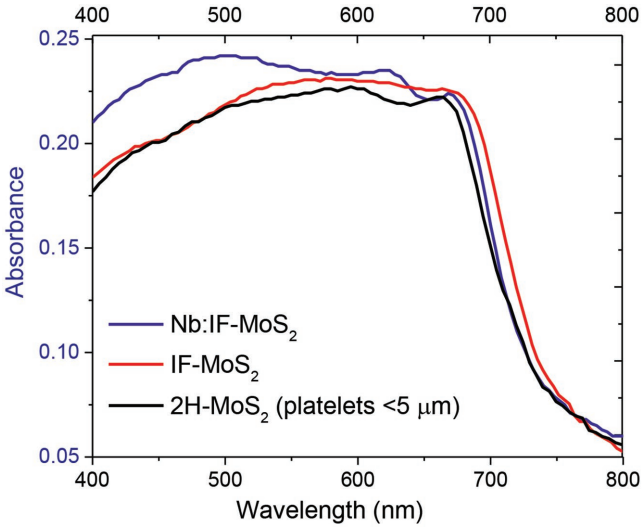

Figure 6. Absolute absorbance spectrum of platelets (black line), undoped (red line), and Nb doped (blue line) IF-MoS_2.

smaller than that of the bulk material.[39,40] The shift could be ascribed to the intralayer structural strains.[41] Furthermore, the Re-doping of the IF nanoparticles was shown to produce a blue shift which was attributed to the Burstein–Moss effect, i.e., to band-filling.[42] The shift of exciton A is smaller compared to the shift of the B exciton, which indicates that the latter is more sensitive to confinement and is strongly perturbed by formation of the IF structure.[43]

Perhaps the most striking difference between the undoped (and Re-doped) NP is the smaller spin–orbit splitting of the Nb-doped IF. This splitting is a manifestation of a higher degeneracy between the heavy and light holes in the valence band.

3.3. Energy Level Schemes of Undoped and Nb Doped IF-MoS_2

Figure 7 shows the qualitative energy level schemes of undoped and Nb doped IF-MoS_2. The derivation of this scheme was based on the Kelvin probe measurements (Sec. 2.2.7) and the optical absorption measurements (Sec. 2.2.8). This energy diagram provides a pictorial rendering of the effect of Nb doping

Table 3. Summary of band gaps, exciton peak positions, and spin–orbit splitting measured for bulk, undoped, and Nb doped IF-MoS_2 (the literature values are given in parentheses).

	Exciton [eV]		Spin–orbit splitting [eV]	Band gap [eV]	
	A	B		Indirect	Direct
Platelets 2H-MoS_2	1.879	2.114	0.235	1.033	1.921
	(1.880[44])	(2.060[44])	(0.180[44])	(1.06[45])	(1.922[44])
IF-MoS_2	1.867	2.081	0.214	1.243	1.909
	(1.846[39])	(2.005[39])	(0.159[39])	–	(1.888[39])
Nb doped IF-MoS_2	1.848	1.994	0.146	1.040	1.890
Re doped IF-MoS_2	1.882	2.082	0.200	1.016	1.924

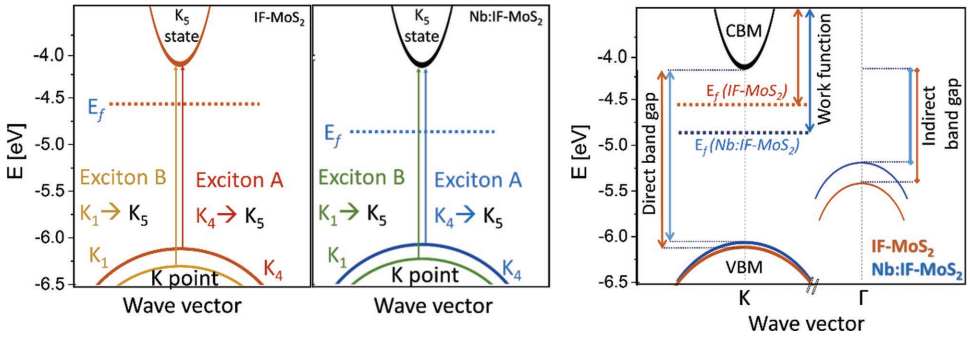

Figure 7. Semi-quantitative energy level schemes of a) undoped and b) Nb doped IF-MoS_2. Here the direct and indirect band gap (BG) were derived using optical measurements (section 2.2.8, 3.2.8) and the Fermi level was derived using the KPFM measurements (section 2.2.7, 3.2.7). Schematic view of the transitions corresponding to excitons A and B. In both panels, excitons A and B are associated with optically allowed $K_4 \rightarrow K_5$ and $K_1 \rightarrow K_5$ transitions. Labels are according to refs. [3,46]. c) Direct comparison between the energy gaps and the work function of undoped and Nb doped IF-MoS_2. The CBM and VBM are conduction band minimum and valence band maximum, correspondingly. The direct BG corresponds to the transition in the K and indirect BG to the Γ point.

on the band structure and the position of the Fermi level. Clearly, doping of the IF-MoS_2 nanoparticles with few hundred ppm of niobium atoms pushes the Fermi level away from the conduction band toward midgap. Nevertheless, full compensation of the n-type characteristic, i.e., making holes the majority carriers has not been achieved.

4. Conclusions

A new strategy was advanced in this work which allowed synthesis of MoS_2 nanoparticles with fullerene-like structure with minute amounts (about 0.1 at%) of niobium as substitutional (p-type) dopant. It was found that the most critical step in successful Nb doping of MoS_2 is the preparation of mixed Nb—Mo—O precursor. Both the use of this precursor and the analysis of the niobium content in the IF nanoparticles by resonance XRF are new in this context. Using XRD and XRF analysis it was shown that Nb^{5+} ions substitute the Mo^{6+} ions in the tetragonal lattice of the oxide precursor. That finding contradicts the previous study of $Nb_2Mo_3O_{14}$ crystal, where substitution of Nb^{5+} ions by Mo^{6+} ions was observed.[35] Hence, the preparation of the precursor is found to be of scientific and technological merit on its own. This precursor was used to prepare the Nb-doped IF-MoS_2 nanoparticles.

Following a detailed analysis, the substitutional nature of the niobium in the MoS_2 lattice and its concentration was confirmed. Using ζ-potential measurements it was shown that the substitutional Nb doping partially "anneals-out" the intrinsic negative surface charge of the IF NP. Furthermore, electrical and optical measurements were performed in order to determine the variation of the Fermi level and band diagram of the Nb doped versus undoped IF-MoS_2 nanoparticles. The influence of the Nb-doping on the physiochemical properties of the nanoparticles, such as rheological and tribological properties, is yet to be investigated.

As doping of semiconductors is a fundamental processes for controlling their properties, the applications of the successful p-type doping of NP are quite broad. Indeed, the Nb doping was already shown to have a beneficial effect in the electrocatalytic hydrogen evolution reaction.[47] Other promising applications of the Nb-doped IF nanoparticles for future investigations are in the field of catalysis, photocatalysis, and tribology. Also, it is believed that in the same vain, inorganic nanotubes of WS_2 and MoS_2 can be Nb-doped, which is supported by a recent experimental work to be published elsewhere.

Supporting Information

Supporting Information is available from the Wiley Online Library or from the author.

Acknowledgements

The authors thank Bat-El Raphael for her help with the Kelvin probe measurements. The authors acknowledge support from the FTA action "Inorganic nanotube-polymer composites" No. 711543 of the Israel National Nano Initiative, the Irving and Cherna Moskowitz Center for Nano and Bio-Nano Imaging grant No. 7208214, and the Perlman Family Foundation; the Israel Science Foundation grants No. 265/12, the Kimmel Center for Nanoscale Science grant No. 43535000350000, the German-Israeli Foundation (GIF) grant No. 712053, the Irving and Azelle Waltcher Foundations in honor of Prof. M. Levy grant No. 720821, the EU project ITN- "MoWSeS" grant No. 317451, the G. M. J. Schmidt Minerva Center for Supramolecular Chemistry grant No. 434000340000. The work of A.I.F. was funded by the Division of Chemical Sciences, Geosciences, and Biosciences, Office of Basic Energy Sciences of the U.S. Department of Energy through Grant DE-FG02- 03ER15476. Work at the X18-A beamline was supported through the Synchrotron Catalysis Consortium (U.S. Department of Energy, Office of Basic Energy Sciences, Grant No. DE-SC0012335.

Conflict of Interest

The authors declare no conflict of interest.

Keywords

doping, fullerene-like, inorganic nanotubes, nanoparticles

Received: May 8, 2017
Revised: July 3, 2017
Published online: December 11, 2017

[1] S. M. Sze, K. K. Ng, *Physics of Semiconductor Devices*, John Wiley & Sons, Hoboken, New Jersey **2006**.
[2] W. Liang, S. Cundy, *Philos. Mag.* **1969**, *19*, 1031.
[3] R. Coehoorn, C. Haas, R. De Groot, *Phys. Rev. B* **1987**, *35*, 6203.
[4] K. Tiong, P. Liao, C. Ho, Y. Huang, *J. Cryst. Growth* **1999**, *205*, 543.
[5] J. Wildervanck, F. Jellinek, *J. Less-Common Met.* **1971**, *24*, 73.
[6] R. Späh, U. Elrod, M. Lux-Steiner, E. Bucher, S. Wagner, *Appl. Phys. Lett.* **1983**, *43*, 79.
[7] L. Yadgarov, R. Rosentsveig, G. Leitus, A. Albu-Yaron, A. Moshkovich, V. Perfilyev, R. Vasic, A. I. Frenkel, A. N. Enyashin, G. Seifert, *Angew. Chem., Int. Ed.* **2012**, *51*, 1148.
[8] A. Sedova, R. Ron, O. Goldbart, O. Elianov, L. Yadgarov, N. Kampf, R. Rosentsveig, D. Shumalinsky, L. Lobik, B. Shay, *Nanomater. Energy* **2015**, *4*, 30.
[9] J. Wilson, A. Yoffe, *Adv. Phys.* **1969**, *18*, 193.
[10] M. Shafer, *Phys. Rev. Lett.* **1972**, *28*, 808.
[11] V. V. Ivanovskaya, A. Zobelli, A. Gloter, N. Brun, V. Serin, C. Colliex, *Phys. Rev. B* **2008**, *78*, 134104.
[12] R. S. Title, M. W. Shafer, *Phys. Rev. Lett.* **1972**, *28*, 808.
[13] M. R. Laskar, D. N. Nath, L. Ma, E. W. Lee, C. H. Lee, T. Kent, Z. Yang, R. Mishra, M. A. Roldan, J.-C. Idrobo, *Appl. Phys. Lett.* **2014**, *104*, 092104.
[14] S. Das, M. Demarteau, A. Roelofs, *Appl. Phys. Lett.* **2015**, *106*, 173506.
[15] J. Suh, T.-E. Park, D.-Y. Lin, D. Fu, J. Park, H. J. Jung, Y. Chen, C. Ko, C. Jang, Y. Sun, *Nano Lett.* **2014**, *14*, 6976.
[16] K. Dolui, I. Rungger, C. D. Pemmaraju, S. Sanvito, *Phys. Rev. B* **2013**, *88*, 075420.
[17] V. V. Ivanovskaya, T. Heine, S. Gemming, G. Seifert, *Phys. Status Solidi B* **2006**, *243*, 1757.
[18] V. V. Ivanovskaya, G. Seifert, A. L. Ivanovskii, *Russ. J. Inorg. Chem.* **2006**, *51*, 320.
[19] F. L. Deepak, H. Cohen, S. Cohen, Y. Feldman, R. Popovitz-Biro, D. Azulay, O. Millo, R. Tenne, *J. Am. Chem. Soc.* **2007**, *129*, 12549.
[20] Y. Yao, L. Tolentino, Z. Yang, X. Song, W. Zhang, Y. Chen, C. p. Wong, *Adv. Funct. Mater.* **2013**, *23*, 3577.
[21] G. Ma, H. Peng, J. Mu, H. Huang, X. Zhou, Z. Lei, *J. Power Sources* **2013**, *229*, 72.
[22] R. Rosentsveig, A. Margolin, A. Gorodnev, R. Popovitz-Biro, Y. Feldman, L. Rapoport, Y. Novema, G. Naveh, R. Tenne, *J. Mater. Chem.* **2009**, *19*, 4368.
[23] L. Yadgarov, C. L. Choi, A. Sedova, A. Cohen, R. Rosentsveig, O. Bar-Elli, D. Oron, H. Dai, R. Tenne, *ACS Nano* **2014**, *8*, 3575.
[24] T. Glatzel, M. C. Lux-Steiner, E. Strassburg, A. Boag, Y. Rosenwaks, *Principles of Kelvin Probe Force Microscopy*, Springer, New York, NY **2007**, pp. 113.
[25] V. Palermo, M. Palma, P. Samorì, *Adv. Mater.* **2006**, *18*, 145.
[26] T. Kittel, E. Roduner, *J. Phys. Chem. C* **2016**, *120*, 8907.
[27] A. Sasahara, C. L. Pang, H. Onishi, *J. Phys. Chem. B* **2006**, *110*, 17584.
[28] S. Itzhakov, H. Shen, S. Buhbut, H. Lin, D. Oron, *J. Phys. Chem. C* **2013**, *117*, 22203.
[29] K. Suzuki, *Nat. Photonics* **2011**, *5*, 316.
[30] P. A. Lee, *Optical and Electrical Properties*, D. Reidel Publishing Company, Dordrecht/Boston **1976**.
[31] P. Afanasiev, *J. Phys. Chem. B* **2005**, *109*, 18293.
[32] P. Afanasiev, L. Fischer, F. Beauchesne, M. Danot, V. Gaborit, M. Breysse, *Catal. Lett.* **2000**, *64*, 59.
[33] T. Ekstrom, M. Nygren, *Acta Chem. Scand.* **1972**, *26*, 1836.
[34] T. Ekstrom, *Acta Chem. Scand.* **1971**, *25*, 2591.
[35] T. Y. Kardash, L. Plyasova, V. Bondareva, A. Shmakov, *J. Struct. Chem.* **2008**, *49*, 701.
[36] M. Newville, *J. Synchrotron Radiat.* **2001**, *8*, 322.
[37] N. Allali, E. Prouzet, A. Michalowicz, V. Gaborit, A. Nadiri, M. Danot, *Appl. Catal., A* **1997**, *159*, 333.
[38] J. Huster, H. Franzen, *J. Less-Common Met.* **1985**, *113*, 119.
[39] G. L. Frey, S. Elani, M. Homyonfer, Y. Feldman, R. Tenne, *Phys. Rev. B* **1998**, *57*, 6666.
[40] L. Scheffer, R. Rosentzveig, A. Margolin, R. Popovitz-Biro, G. Seifert, S. Cohen, R. Tenne, *Phys. Chem. Chem. Phys.* **2002**, *4*, 2095.
[41] Q. C. Sun, X. Xu, L. Vergara, R. Rosentsveig, J. Musfeldt, *Phys. Rev. B* **2009**, *79*, 205405.
[42] Q. C. Sun, L. Yadgarov, R. Rosentsveig, G. Seifert, R. Tenne, J. L. Musfeldt, *ACS Nano* **2013**, *7*, 3506.
[43] I. McGovern, R. Williams, C. Mee, *Surf. Sci.* **1974**, *46*, 427.
[44] J. V. Acrivos, W. Liang, J. Wilson, A. Yoffe, *J. Phys. C: Solid State Phys.* **1971**, *4*, L18.
[45] H. S. S. Ramakrishna Matte, A. Gomathi, A. K. Manna, D. J. Late, R. Datta, S. K. Pati, C. N. R. Rao, *Angew. Chem.* **2010**, *122*, 4153.
[46] T. Böker, R. Severin, A. Müller, C. Janowitz, R. Manzke, D. Voß, P. Krüger, A. Mazur, J. Pollmann, *Phys. Rev. B* **2001**, *64*, 235305.
[47] M. Chhetri, U. Gupta, L. Yadgarov, R. Rosentsveig, R. Tenne, C. Rao, *ChemElectroChem* **2016**, *3*, 1937.

